Research Article | Vol. 25, No. 24 | 27 Nov 2017 | OPTICS EXPRESS 30149
Optics EXPRESS

Quantum memory and non-demolition measurement of single phonon state with nitrogen-vacancy centers ensemble

RUI-XIA WANG,[1] KANG CAI,[1] ZHANG-QI YIN,[2,3] AND GUI-LU LONG[1,*]

[1] *State Key Laboratory of Low-dimensional Quantum Physics and Department of Physics, Tsinghua University, Beijing 100084, China*
[2] *Center for Quantum Information, Institute for Interdisciplinary Information Sciences, Tsinghua University, Beijing 100084, China*
[3] *yinzhangqi@tsinghua.edu.cn*
[*] *gllong@tsinghua.edu.cn*

Abstract: In a diamond, the mechanical vibration-induced strain can lead to interaction between the mechanical mode and the nitrogen-vacancy (NV) centers. In this work, we propose to utilize the strain-induced coupling for the quantum non-demolition (QND) single phonon measurement and memory in a diamond. The single phonon in a diamond mechanical resonator can be perfectly absorbed and emitted by the NV centers ensemble (NVE) with adiabatically tuning the microwave driving. An optical laser drives the NVE to the excited states, which have much larger coupling strength to the mechanical mode. By adiabatically eliminating the excited states under large detuning limit, the effective coupling between the mechanical mode and the NVE can be used for QND measurement of the single phonon state. Under realistic experimental conditions, we numerically simulate the scheme. It is found that the fidelity of the absorbing and emitting process can reach a much high value. The overlap between the input and the output phonon shapes can reach 98.57%.

OCIS codes: (270.5570) Quantum detectors; (230.4685) Optical microelectromechanical devices; (220.4880) Optomechanics.

References and links

1. L. M. Duan, M. D. Lukin, I. Cirac, and P. Zoller, "Long-distance quantum communication with atomic ensembles and linear optics," Nature **414**, 413–418 (2001).
2. Z. Q. Yin and F. L. Li, "Multiatom and resonant interaction scheme for quantum state transfer and logical gates between two remote cavities via an optical fiber," Phys. Rev. A **75**, 012324 (2007).
3. C. Song, K. Xu, W. Liu, C. Yang, S. B. Zheng, H. Deng, Q. Xie, K. Huang, Q. Guo, L. Zhang, P. Zhang, D. Xu, D. Zheng, X. Zhu, H. Wang, Y. A. Chen, C. Y. Lu, S. Han, and J. W. Pan, "10-qubit entanglement and parallel logic operations with a superconducting circuit," https://arxiv.org/abs/1703.10302 (2017).
4. Q. Hou, W. Yang, C. Chen, and Z. Yin, "Electromagnetically induced acoustic wave transparency in a diamond mechanical resonator," J. Opt. Soc. Am. B **33**, 2242–2250 (2016).
5. X. Wang, A. Miranowicz, H. R. Li, and F. Nori, "Method for observing robust and tunable phonon blockade in a nanomechanical resonator coupled to a charge qubit," Phys. Rev. A **93**, 063861 (2016).
6. V. M. Stojanovic, M. Vanevic, E. Demler, and L. Tian, "Transmon-based simulator of nonlocal electron-phonon coupling: a platform for observing sharp small-polaron transitions," Phys. Rev. B **89**, 144508 (2014).
7. A. D. O'Connell, M. Hofheinz, M. Ansmann, R. C. Bialczak, M. Lenander, E. Lucero, M. Neeley, D. Sank, H. Wang, M. Weides, J. Wenner, J. M. Martinis, and A. N. Cleland, "Quantum ground state and single-phonon control of a mechanical resonator," Nature **464**, 697–703 (2010).
8. T. Li and Z. Q. Yin, "Quantum superposition, entanglement, and state teleportation of a microorganism on an electromechanical oscillator," Sci. Bull. **61**, 163–171 (2016).
9. M. J. A. Schuetz, E. M. Kessler, G. Giedke, L. M. K. Vandersypen, M. D. Lukin, and J. I. Cirac, "Universal Quantum Transducers Based on Surface Acoustic Waves," Phys. Rev. X **5**, 031031 (2015).
10. P. Arrangoiz-Arriola and A. H. Safavi-Naeini, "Engineering interactions between superconducting qubits and phononic nanostructures," Phys. Rev. A **94**, 063864 (2016).

#306755 https://doi.org/10.1364/OE.25.030149
Journal © 2017 Received 11 Sep 2017; revised 6 Nov 2017; accepted 6 Nov 2017; published 16 Nov 2017

Optics EXPRESS

11. M. V. Gustafsson, T. Aref, A. F. Kockum, M. K. Ekström, G. Johansson, and P. Delsing, "Propagating phonons coupled to an artificial atom," Science **346**, 207–211 (2014).
12. S. M. Meenehan, J. D. Cohen, G. S. MacCabe, F. Marsili, M. D. Shaw, and O. Painter, "Position-squared coupling in a tunable photonic crystal optomechanical cavity," Phys. Rev. X **5**, 041002 (2015).
13. R. Manenti, A. F. Kockum, A. Patterson, T. Behrle, J. Rahamim, G. Tancredi, F. Nori, and P. J. Leek, "Circuit quantum acoustodynamics with surface acoustic waves," https://arxiv.org/abs/1703.04495 (2017).
14. C. Galland, N. Sangouard, N. Piro, N. Gisin, and T. J. Kippenberg, "Heralded single-phonon preparation, storage, and readout in cavity optomechanics," Phys. Rev. Lett. **112**, 143602 (2014).
15. O. Matsuda, O. B. Wright, D. H. Hurley, V. Gusev, and K. Shimizu, "Coherent shear phonon generation and detection with picosecond laser acoustics," Phys. Rev. B **77**, 224110 (2008).
16. O. Matsuda, O. B.Wright, D. H. Hurley, V. E. Gusev, and K. Shimizu, "Coherent Shear Phonon Generation and Detection with Ultrashort Optical Pulses," Phys. Rev. Lett. **93**, 095501 (2004).
17. Y. Yanay and A. A. Clerk, "Shelving-style phonon-number detection in quantum optomechanics," New J. Phys. **19**, 033014 (2017).
18. J. H. Chai and Y. Q. Lu, "Effects of phase mismatch and losses on phonon squeezing and quantum nondemolition measurements in detection of hypersonic phonons by squeezed light," Physica B **291**, 292–298 (2000).
19. X. Baia, T. A. Eckhausea, S. Chakrabartib, P. Bhattacharyab, R. Merlina, and C. Kurdak, "Phonon detection using quasi one-dimensional quantum wires," Physica E **34**, 592–595 (2006).
20. M. J. Woolley, A. C. Doherty, and G. J. Milburn, "Continuous quantum non-demolition measurement of Fock states of a nanoresonator using feedback-controlled circuit QED," Phys. Rev. B **82**, 094511 (2010).
21. C. Ohm, C. Stampfer, J. Splettstoesser, and M. R. Wegewijs, "Readout of carbon nanotube vibrations based on spin-phonon coupling," Appl. Phys. Lett. **100**, 143103 (2012).
22. O. P. deSaNeto, M. C. deOliveira, F. Nicacio, and G. J. Milburn, "Capacitive Coupling of Two Transmission Line Resonators Mediated by the Phonon Number of a Nanoelectromechanical Oscillator," Phys. Rev. A **90**, 023843 (2014).
23. S. Gleyzes, S. Kuhr, C. Guerlin, J. Bernu, S. Deléglise, U. B. Hoff, M. Brune, J. M. Raimond, and S. Haroche, "Quantum jumps of light recording the birth and death of a photon in a cavity," Nature **446**, 297–300 (2007).
24. M. Eichenfield, J. Chan, R. M. Camacho, K. J. Vahala, and O. Painter, "Optomechanical crystals," Nature **462**, 78–82 (2009).
25. Y. Liu, F. Kong, F. Shi, and J. Du, "Detection of radio-frequency field with a single spin in diamond," Sci. Bull. **61**, 1132 (2016).
26. P. Ovartchaiyapong, K. W. Lee, B. A. Myers, and A. C. B. Jayich, "Dynamic strain-mediated coupling of a single diamond spin to a mechanical resonator," Nat. Commun. **5**, 4429 (2014).
27. D. A. Golter, T. Oo, M. Amezcua, K. A. Stewart, and H. Wang, "Optomechanical Quantum Control of a Nitrogen-Vacancy Center in Diamond," Phys. Rev. Lett. **116**, 143602 (2016).
28. E. R. MacQuarrie, M. Otten, S. K. Gray, and G. D. Fuchs, "Cooling a mechanical resonator with nitrogen-vacancy centres using a room temperature excited state spin-strain interaction," Nat. Commun. **8**, 14358 (2017).
29. P. Rabl, P. Cappellaro, M. V. G. Dutt, L. Jiang, J. R. Maze, and M. D. Lukin, "Strong magnetic coupling between an electronic spin qubit and a mechanical resonator," Phys. Rev. B **79**, 041302 (2008).
30. P. Rabl, S. J. Kolkowitz, F. H. L. Koppens, J. G. E. Harris, P. Zoller, and M. D. Lukin, "A quantum spin transducer based on nanoelectromechanical resonator arrays," Nat. Phys. **6**, 602–608 (2010).
31. Z. Y. Xu, Y. M. Hu, W. L. Yang, M. Feng, and J. F. Du, "Deterministically entangling distant nitrogen-vacancy centers by a nanomechanical cantilever," Phys. Rev. A **80**, 022335 (2009).
32. L. G. Zhou, L. F. Wei, M. Gao, and X. B. Wang, "Strong coupling between two distant electronic spins via a nanomechanical resonator," Phys. Rev. A **81**, 042323 (2010).
33. Z. Q. Yin, T. C. Li, X. Zhang, and L. M. Duan, "Large quantum superpositions of a levitated nanodiamond through spin-optomechanical coupling," Phys. Rev. A **88**, 033614 (2013).
34. Y. Ma, Z. Q. Yin, P. Huang, W. L. Yang, and J. F. Du, "Cooling a Mechanical Resonator to Quantum Regime by heating it," Phys. Rev. A **94**, 053836 (2016).
35. K. Cai, R. X. Wang, Z. Q. Yin, and G. L. Long, "Second-order magnetic field gradient-induced strong coupling between nitrogen-vacancy centers and a mechanical oscillator," Sci. China Phys. Mech. **60**, 070311 (2017).
36. S. D. Bennett, N. Y. Yao, J. Otterbach, P. Zoller, P. Rabl, and M. D. Lukin, "Phonon-induced spin-spin interactions in diamond nanostructures: application to spin squeezing," Phys. Rev. Lett. **110**, 156402 (2013).
37. D. A. Golter, T. Oo, M. Amezcua, I. Lekavicius, K. A. Stewart, and H. Wang, "Coupling a Surface Acoustic Wave to an Electron Spin in diamond via a Dark State," Phys. Rev. X **6**, 041060 (2016).
38. D. A. Golter, T. Oo, M. Amezcua, K. A. Stewart, and H. Wang, "Optomechanical Quantum Control of a Nitrogen-Vacancy Center in Diamond," Phys. Rev. Lett. **116**, 143602 (2016).
39. J.R. Maze, A. Gali, E. Togan, Y. Chu, A. Trifonov, E. Kaxiras, and M. D. Lukin, "Properties of nitrogen-vacancy centers in diamond: group theoretic approach," New J. Phys. **13**, 025025 (2011).
40. M. W. Doherty, N. B. Manson, P. Delaney, and L. C. L. Hollenberg, "The negatively charged nitrogen-vacancy centre in diamond: the electronic solution," New J. Phys. **13**, 025019 (2011).
41. V. B. Braginsky and F. Y. Khalili, Quantum Measurement, Cambridge Univ. Press, 1992.
42. P. Grangier, J. A. Levenson, and J. P. Poizat, "Quantum non-demolition measurements in optics," Nature **396**, 537–542

Optics EXPRESS

(1998).
43. G. Nogues, A. Rauschenbeutel, S. Osnaghi, M. Brune, J. M. Raimond, and S. Haroche, "Seeing a single photon without destroying it," Nature **400**, 239–242 (1999).
44. N. B. Manson, J. P. Harrison, and M. J. Sellars, "Nitrogen-vacancy center in diamond: Model of the electronic structure and associated dynamics," Phys. Rev. B **74**, 104303 (2006).
45. S. Saito, X. Zhu, R. Amsüss, Y. Matsuzaki, K. Kakuyanagi, T. Shimo-Oka, N. Mizuochi, K. Nemoto, W. J. Munro, and K. Semba, "Towards realizing a quantum memory for a superconducting qubit: storage and retrieval of quantum states," Phys. Rev. Lett. **111**, 107008 (2013).
46. L. J. Rogers, S. Armstrong, M. J. Sellars, and N. B. Manson, "Infrared emission of the NV centre in diamond: Zeeman and uniaxial stress studies," New J. Phys. **10**, 103024 (2008).
47. Z. Yin, N. Zhao, and T. Li, "Hybrid opto-mechanical systems with nitrogen-vacancy centers," Sci. China Phys. Mech. **58**, 050303 (2015).
48. L. M. Duan, A. Kuzmich, and H. J. Kimble, "Cavity QED and quantum-information processing with "hot" trapped atoms," Phys. Rev. A **67**, 032305 (2003).
49. Z. Yin, W. L. Yang, L. Sun, and L. M. Duan, "Quantum network of superconducting qubits through opto-mechanical interface," Phys. Rev. A **91**, 012333 (2015).
50. J. I. Cirac, P. Zoller, H. J. Kimble, and H. Mabuchi, "Quantum state transfer and entanglement distribution among distant nodes in a quantum network," Phys. Rev. Lett. **78**, 3221–3224 (1997).
51. D. F. V. James and J. Jerker, "Effective hamiltonian theory and its applications in quantum information," Can. J. Phys. **85**, 625–632 (2007).
52. L. Robledo, H. Bernien, V. D. S. Toeno, and R. Hanson, "Spin dynamics in the optical cycle of single nitrogen-vacancy centres in diamond," New J. Phys. **13**, 025013 (2010).
53. N. Bar-Gill, L.M. Pham, A. Jarmola, D. Budker, and R.L. Walsworth, "Solid-state electronic spin coherence time approaching one second," Nat. Commun. **4**, 1743 (2013).
54. Y. Tao, J. M. Boss, B. A. Moores, and C. L. Degen, "Single-crystal diamond nanomechanical resonators with quality factors exceeding one million," Nat. Commun. **5**, 3638 (2014).

1. Introduction

In quantum information processing, one of the key challenges is to realize the effective coupling, or communication, between distant qubits. Usually, the photon is used as flying qubit for quantum communications [1], or inducing the effective coupling between the distant qubits [2]. For example, in superconducting quantum circuit systems, the microwave photon confined in transmission lines resonator is used as a quantum bus [3]. Recently, with the advances in the fabrication and manipulation of the mechanical systems [4–8], an alternative way of using phonon to couple distant qubits was proposed [9]. The surface acoustic wave (SAW) has been successfully coupled with superconducting qubits [10, 11]. The advantages of the phonon quantum bus compared with the photon quantum bus are the high quality factor and small effective size [9, 10, 12]. The speed of SAW is 5 orders of magnitude slower than the speed of light [11, 13]. Therefore, the wavelength of SAW at GHz is also 5 orders of magnitude smaller than the microwave light. In this way, the individual superconducting qubit addressing by SAW is possible. There are many schemes concerning single phonons, for example, the phonon states preparation [14–16], detection [14–21], and the phonon mediated interface [22].

As we know, in quantum optics experiments, the single photon detectors are widely used. For microwave photons, the quantum non-demolition (QND) measurement for photon number states have been realized in both cavity QED and superconducting circuit QED systems [23]. The QND measurement in circuit QED systems can be used for quantum error corrections. In order to further develop the phonon based quantum information processing, the efficient single phonon detector is needed. The ultimate goal is to realize QND measurement on single phonon state. Inspired by the QND measurement for photon number states, we use the strain induced phonon and the NVE coupling in the diamond to get the strong nonlinearity for the QND measurement of the single phonon state. The geometry of the mechanical crystal structure contains a diamond crystal with rectangular holes arranged periodically which can precisely manipulate mechanical vibrations [24].

The nitrogen-vacancy (NV) center, which consists a substitutional nitrogen atom and adjacent vacancy in diamond, is one of the most promising system for solid-state quantum information

Optics EXPRESS

processing. NV centers can be controlled by microwave with long coherence time even at room temperature [25]. The diamond lattice vibration, or phonon, can couple with the NV centers ensemble (NVE) [26, 27] and be cooled by the NVE [28]. There are two different kind of mechanism for coupling the NV center and the phonons. The first one is magnetic field induced coupling [29–35], and the second one is the strain induced coupling [36–38]. Here we focus on the second method. The strain induced coupling between NV centers electron spins in the ground state and the phonons is usually quite small, e.g. several kHz [36]. Recently, the excited-state electron-phonon coupling has been reported in experiments [38]. It is about 6 orders of magnitude stronger than the ground-state electron-phonon coupling [39, 40]. By taking the advantage of strong coupling, the quantum control of the internal states of a NV center has been realized by using optomechanical sideband transition [38]. We can use this strong coupling mechanism to induce the strong effective nonlinear coupling between the phonon and the NVE, and realized QND phonon number measurement.

In this work, the strain-induced spin-phonon coupling is employed in designing the scheme for the single phonon absorption, emission and QND measurement. We consider the NVE situated a few μm below the diamond surface which is shown in Fig. 1(a). The coupling strength between the NVE and the single phonon can be enhanced by a factor $\sqrt{N}$ through the collective excitation, which can reach the strong coupling regime. The resonant frequency of the phonons propagating in the diamond can be controlled by the rectangular holes shown in the upper diagram of Fig. 1(a), which are periodically arranged on the diamond chip. We may assume that, the resonant frequency of the diamond chip is ω_m. Then, our proposed scheme can be implemented by four steps. The first step is initialization. In this step, all of the NV centers are prepared to state $|-1\rangle$. In the second step, the single phonon with the resonant frequency ω_m can be absorbed by the NVE, and the absorption will induce the resonant frequency shift which can be revealed in the phonon absorption spectrum. In step three, we can detect the single phonon state through probing the resonance frequency shift of the phonons in the diamond. The final step is the inverse process of the single phonon detection. In this step, the absorbed single phonon is emitted. The emitted phonon shape can be controlled by regulating the driving pulse acting on the NVE. The similarity between the emitted and the absorbed single phonon reaches 98.57% if we inverse the driving pulse when emitting compared with the absorbing process. If the single phonon state is in quantum state before absorbing, the size and shape of the phonon will not be changed when emitting, this process is a quantum non-demolition (QND) measurement process, which realizes an ideal projective measurement that leaves the system in an eigenstate of the phonon number [23, 41–43].

2. Model

As schematically shown in Fig. 1(a), we consider a diamond chip with periodically arranged rectangle holes to adjust the refractive index for the surface acoustic wave (SAW). The NVE are located near the diamond surface coupling to the laser, microwave and SAW.

With a zero magnetic field, the spin-triplet ground state of the NV center splits into two energy levels, $M_s = 0$ and the nearly degenerate sublevels $M_s = \pm 1$ [44]. We apply an external magnetic field $\overrightarrow{B}_{ext}$ along the crystalline direction [100] of the NV center [45] to split the degenerate sublevels $M_s = \pm 1$, which results in a three-level system denoted by $|0\rangle = |^3A, M_s = 0\rangle$, $|-1\rangle = |^3A, M_s = -1\rangle$, $|+1\rangle = |^3A, M_s = +1\rangle$, respectively. The frequency splitting between the levels $|-1\rangle$ and $|+1\rangle$ is denoted as ω_e. $|E\rangle$ is an excited state with an energy gap of about 1.189eV to the ground state [46]. The schematic diagram of the NV center energy structure is shown in Fig. 1(b).

The NV centers exist in a diamond crystal and they can sense the lattice vibrations. If there is a phonon produced in the lattice, the NV center can absorb it when the mechanical frequency and the energy splitting of the NV centers are matched [36, 47]. For this system, the phonon mode

Optics EXPRESS

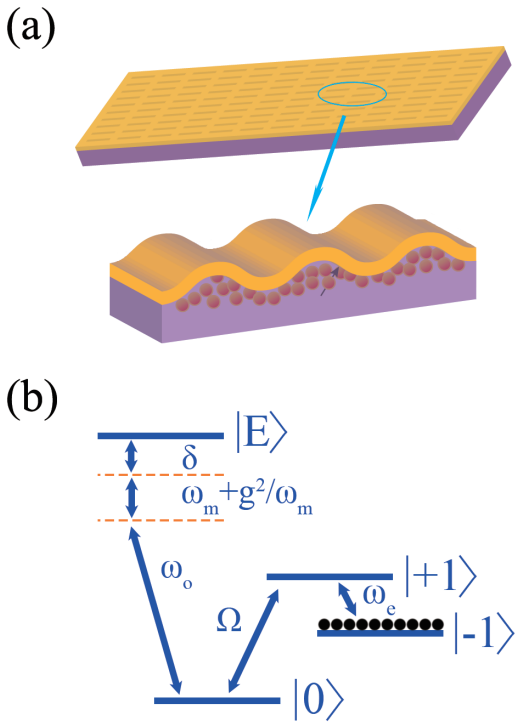

Fig. 1. (a) A schematic diagram of the phononic crystal. The NVE located near the surface coupling to a single phonon and a laser field. (b) The electronic structure of the NV center. Ω is the Rabi frequency between the energy levers $|0\rangle$ and $|+1\rangle$ induced by the microwave drive. ω_m is the phonon mode. ω_o is the optical driving frequency between the energy levels $|0\rangle$ and $|E\rangle$ inducing the Rabi frequency of Ω_o.

a_m with the frequency ω_m couples to the NV centers with transition of $|-1\rangle$ to $|+1\rangle$. We can adjust the external magnetic field $\overrightarrow{B}_{ext}$ to make the frequency ω_e equal to ω_m and the phonon modes propagating in the free space in diamond with the frequency ω are denoted by $e(\omega)$ which can couple to the phonon mode a_m. A classical microwave field $\varepsilon(t) = \widetilde{\varepsilon}(t)\, e^{-i\omega_{01}t}$ drives the transition $|+1\rangle$ to $|0\rangle$ with a Rabi oscillation frequency $\Omega(t)$ (ω_{01} is the frequency splitting between the levels $|0\rangle$ and $|+1\rangle$). The Rabi frequency $\Omega(t)$ can be written as $\Omega(t) = \Omega_0 \alpha(t)$. Within a good approximation, we assume that $\widetilde{\varepsilon}(t)$ increase gradually from zero with $\widetilde{\varepsilon}(0) \simeq 0$ to a finite strength. Because $\alpha(t)$ is proportional to $\widetilde{\varepsilon}(t)$ ($\alpha(t) \propto \widetilde{\varepsilon}(t)$), then we can get $\Omega(t) = \Omega_0' \widetilde{\varepsilon}(t)$, which describes that the shape of the amplitude of the classical driving microwave field totally decides the Rabi frequency.

Neglecting the dissipation of the NVE system, the Hamiltonian of the NVE system including

Optics EXPRESS

the coupling between the mode a_m and the output can be written as (setting $\hbar = 1$) [48,49]

$$\begin{aligned} H = & \sum_{i=1}^{N} G_m(|+1\rangle_i\langle -1|a_m + |-1\rangle_i\langle +1|a_m^\dagger) \\ & + \frac{\Omega(t)}{2}\sum_{i=1}^{N}(|0\rangle_i\langle +1| + |+1\rangle_i\langle 0|) \\ & + i\sqrt{\kappa/2\pi}\int_{+\Delta\omega_e}^{+\Delta\omega_e} d\omega[a_m^\dagger e(\omega) - a_m e^\dagger(\omega)] \\ & + \int_{+\Delta\omega_e}^{+\Delta\omega_e} d\omega[\omega e^\dagger(\omega)e(\omega)]. \end{aligned} \tag{1}$$

where G_m is the coupling rate between single NV center and the phonon, which is typically small. We need to consider the free propagating modes within a finite bandwidth $[\omega_e - \Delta\omega_e, \omega_e + \Delta\omega_e]$ that couple to the NV mode with the carrier frequency ω_e. Within this bandwidth, the coupling between $e(\omega)$ and the NV is a constant approximately which is denoted by $\sqrt{\kappa/2\pi}$ for convenience. κ is the effective decay rate.

To obtain the relationship between the driving pulse shape and the output phonon pulse shape, a simple picture by neglecting the dissipation of the NVE system and the coupling of the mode a_m to the output is studied. Initially, the NVE are cooled to the ground state $|0\rangle$, and a π pulse is driven between the state $|0\rangle$ and $|-1\rangle$, and then the NVE is in $|-1\rangle^{\otimes N}$. To increase the accuracy of the initialization in experiment, we can also realize it using an adiabatic process from state $|0\rangle$ to $|-1\rangle$, this adiabatic process is similar with the phonon emission process, which will be described detailedly in section 3 and 5. In the rotating frame, the Hamiltonian of the NVE system is

$$\begin{aligned} H' = & \sum_{i=1}^{N} G_m(|+1\rangle_i\langle -1|a_m + |-1\rangle_i\langle +1|a_m^\dagger) \\ & + \frac{\Omega(t)}{2}\sum_{i=1}^{N}(|0\rangle\langle +1| + |+1\rangle\langle 0|). \end{aligned} \tag{2}$$

We map the operator $|+1\rangle_i\langle -1|$ to the bosonic operators. $\sqrt{N}a^\dagger = \sum_{i=1}^{N}|+1\rangle_i\langle -1|$, $a^\dagger a|n\rangle_{+1} = n|n\rangle_{+1}$ means there are n NVs that are in the state $|+1\rangle$. $d^\dagger = |0\rangle_i\langle +1|$ and $d = |+1\rangle_i\langle 0|$ are the creation and annihilation operators for the ith NV center, and then the Hamiltonian can be written as follow, where $g_m = \sqrt{N}G_m$.

$$H' = g_m(a^\dagger a_m + a a_m^\dagger) + \frac{\Omega(t)}{2}(d^\dagger + d). \tag{3}$$

In the bases of $|N\rangle_{-1}|0\rangle_{+1}|0\rangle_0|1\rangle_m$, $|N-1\rangle_{-1}|1\rangle_{+1}|0\rangle_0|0\rangle_m$, $|N-1\rangle_{-1}|0\rangle_{+1}|1\rangle_0|0\rangle_m$, where the state $|p\rangle_{-1}|q\rangle_{+1}|r\rangle_0|s\rangle_m$ represents that the numbers of the NVs which are in the states $|-1\rangle$, $|+1\rangle$, and $|0\rangle$ are p, q and r respectively, and the number of phonons in the diamond is s. The Hamiltonian can be written as a matrix as follow in the three bases,

$$H' = \begin{bmatrix} 0 & g_m & 0 \\ g_m & 0 & \frac{\Omega(t)}{2} \\ 0 & \frac{\Omega(t)}{2} & 0 \end{bmatrix}. \tag{4}$$

This Hamiltonian has the well-known dark state $|D\rangle$ with the form $|D\rangle = \frac{-\Omega(t)/2}{\sqrt{g_m^2+[\Omega(t)/2]^2}}|N\rangle_{-1}|0\rangle_{+1}|0\rangle_0|1\rangle_m + \frac{g_m}{\sqrt{g_m^2+[\Omega(t)/2]^2}}|N-1\rangle_{-1}|0\rangle_{+1}|1\rangle_0|0\rangle_m$. The dark state means,

Optics EXPRESS

the state will remain on the state $|D\rangle$, if the driving pulse $\Omega(t)$ and the coupling strength satisfy the relationship $\cos\theta = \frac{\Omega(t)/2}{\sqrt{g_m^2+[\Omega(t)/2]^2}}$ and $\sin\theta = \frac{g_m}{\sqrt{g_m^2+[\Omega(t)/2]^2}}$.

The effects of non-zero dissipation will be analyzed in section 5, where the phonon detecting efficiency is calculated as well as the overlap of the absorbing and emitting a single phonon with the real lossy system.

3. Pulse shape

To obtain the relationship of the pulse shape between the driving and the phonon, we first consider the emitting process from state $|N-1\rangle_{-1}|0\rangle_{+1}|1\rangle_0|0\rangle_m$ to $|N\rangle_{-1}|0\rangle_{+1}|0\rangle_0|1\rangle_m$ under ideal conditions. The Hamiltonian of the system can be written as

$$\begin{aligned} H &= g_m\left(a^\dagger a_m + a a_m^\dagger\right) + \frac{\Omega(t)}{2}(d^\dagger + d) \\ &\quad + i\sqrt{\kappa/2\pi}\int_{-\Delta\omega_e}^{+\Delta\omega_e} d\omega\left[a_m^\dagger e(\omega) - a_m e^\dagger(\omega)\right] \\ &\quad + \int_{-\Delta\omega_e}^{+\Delta\omega_e} d\omega\left[\omega e^\dagger(\omega)\, e(\omega)\right]. \end{aligned} \tag{5}$$

Assume that, at the time $t = 0$, the Rabi frequency $\Omega(t) = 0$, the NVE system are in the state $|N-1\rangle_{-1}|0\rangle_{+1}|1\rangle_0|0\rangle_m$, after applying a classical driving pulse $\varepsilon(t)$, the Rabi frequency, which is proportional to the intensity of the driving pulse, changes slowly and is within the adiabatic approximation. Then we can expend the state $|\Psi\rangle$ of the whole system into the following form [48]

$$|\Psi\rangle = c_d|D\rangle \otimes |\phi_0\rangle + |N\rangle_{-1}|0\rangle_{+1}|0\rangle_0|0\rangle_m \otimes |\phi_1\rangle, \tag{6}$$

where $|\phi_0\rangle$ denotes the vacuum state of mode $e(\omega)$ in the diamond, and

$$|\phi_1\rangle = \int_{-\Delta\omega_e}^{+\Delta\omega_e} d\omega c_\omega e^\dagger(\omega)\,|\phi_0\rangle, \tag{7}$$

represents the single phonon output state. Initially, $c_d = 1$, $c_\omega = 0$ and $\Omega(0) = 0$. Within the adiabatic approximation, we would like to calculate the time evolution of the whole NVE system state $|\Psi\rangle$ by substituting it into the schrödinger equation $i\partial_t|\Psi\rangle = H|\Psi\rangle$. The coefficients c_d and c_ω can be got, which satisfy the following evolution equations:

$$\dot{c_d} = \left(-\sqrt{\kappa/2\pi}\cos\theta\right)\int_{-\Delta\omega_e}^{+\Delta\omega_e} c_\omega d\omega, \tag{8}$$

$$\dot{c_\omega} = -i\omega c_\omega + \sqrt{\kappa/2\pi}c_d\cos\theta. \tag{9}$$

We can get the solution of c_ω as follow

$$c_\omega(t) = \sqrt{\kappa/2\pi}\int_0^t e^{-i\omega(t-\tau)}c_d(\tau)\cos\theta(\tau)\,d\tau, \tag{10}$$

substituting the solution into the equation of c_d, leads to

$$\dot{c_d} = -\frac{\kappa\cos\theta}{\pi}\int_0^t \frac{\sin[\delta\omega(t-\tau)]}{(t-\tau)}c_d(\tau)\cos\theta(\tau)\,d\tau. \tag{11}$$

The bandwidth $\delta\omega$ satisfies $\delta\omega T \gg 1$, where the operation time T characterizes the time scale for a significant change of c_d and $\sin\theta$, so the above function satisfies a δ function

$$\delta(x) = \lim_{k\to\infty}\frac{1}{\pi}\frac{\sin kx}{x}, \tag{12}$$

Optics EXPRESS

then we can obtain

$$\dot{c_d} = -\frac{\kappa}{2} c_d(t) \cos^2\theta. \tag{13}$$

The solutions of c_d and c_ω are

$$c_d = e^{-\frac{\kappa}{2}\int_0^t \cos^2\theta(\tau)d\tau}, \tag{14}$$

$$\begin{aligned} c_\omega(t) &= \sqrt{\kappa/2\pi}\int_0^t e^{-i\omega(t-\tau)} e^{-\frac{\kappa}{2}\int_0^t \cos^2\theta(\tau)d\tau} \\ &\quad \cdot cos\theta(\tau)\, d\tau. \end{aligned} \tag{15}$$

The single-phonon pulse shape $f(t)$ can be obtained by the Fourier transformation

$$f(t) = \frac{1}{\sqrt{2\pi}}\int_{-\Delta\omega_e}^{+\Delta\omega_e} d\omega c_\omega(T)\, e^{-i\omega(t-T)} \tag{16}$$

$$= \sqrt{\kappa}\cos\theta(t)\, e^{-\frac{\kappa}{2}\int_0^t \cos^2\theta(\tau)d\tau}. \tag{17}$$

If the Rabi frequency $\Omega(t)$, which is proportional to the strength of the driving pulse, satisfies the function as $\Omega(t) = 2g_m \exp\left[\kappa\left(t-\frac{T}{2}\right)/2\right]$, the output phonon shape will be symmetric. The output phonon shape function can be figured out as

$$f(t) = \frac{\sqrt{\kappa}\sqrt{1+\exp\left(-\frac{\kappa T}{2}\right)}}{\exp\left[-\kappa\left(t-\frac{T}{2}\right)/2\right] + \exp\left[\kappa\left(t-\frac{T}{2}\right)/2\right]}, \tag{18}$$

the results is shown in Fig. 2 for $\kappa/2\pi = 1.6\times10^5$, $T = \frac{20}{\kappa}$. We assume that, in the absorption process, we know the phonon shape in advance, such as the shape in Fig. 2. As the absorption process is the time reversal of the emission process, and the phonon shape is symmetrical in the time domain, if we reverse the temporal driving pulse shape on NV centers in the absorbing process, the phonon can be completely absorbed by the NVE [50]. If the phonon shape is not symmetrical in the time domain, it can also be completely absorbed as long as it is reversed simultaneously with the driving pulse.

4. QND measurement

As schematically shown in Fig. 1(b), we consider the energy levels $|0\rangle$ and $|E\rangle$. After the absorption process, we stop the microwave driving pulse Ω between the state $|0\rangle$ and $|+1\rangle$ and change the external magnetic field intensity to regulate the frequency splitting ω_e to be far detuning, therefore, the ground state spin-phonon interaction can be neglected. At the same time, we start the driving pulse Ω_o between the state $|0\rangle$ and $|E\rangle$ to detect the single phonon state.

The Hamiltonian of the detecting system is

$$\begin{aligned} H &= \omega_m a_m^\dagger a_m + \omega_{0E}|E\rangle\langle E| \\ &\quad + \frac{\Omega_o}{2}\left(e^{i\omega_o t}|0\rangle\langle E| + e^{-i\omega_o t}|E\rangle\langle 0|\right) \\ &\quad + g\left(a_m^\dagger + a_m\right)|E\rangle\langle E|. \end{aligned} \tag{19}$$

Applying the Schrieffer-Wolff transformation

$$U = \exp[\frac{g}{\omega_m}\left(a_m^\dagger - a_m\right)|E\rangle\langle E|]$$

Optics EXPRESS

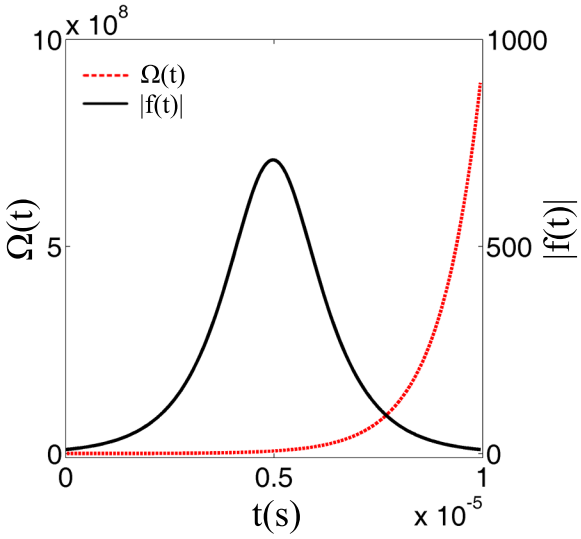

Fig. 2. The situation of the symmetric output phonon shape. The red line is the driving pulse shape applying to the NVE, and the black line represents the pulse shape of the output phonon.

to the Hamiltonian gives

$$\begin{aligned}\widetilde{H} &= UHU^{\dagger} \\ &= \omega_m a_m^{\dagger} a_m - \frac{g^2}{\omega_m}|E\rangle\langle E| + \omega_{0E}|E\rangle\langle E| \\ &\quad + \frac{\Omega_o}{2}[e^{i\omega_o t - \frac{g}{\omega_m}(a_m^{\dagger} - a_m)}|0\rangle\langle E| + H.c.].\end{aligned} \tag{20}$$

Apply the RWA, and set $H_0 = \omega_m a_m^{\dagger} a_m + (\omega_{0E} - \frac{g^2}{\omega_m} - \delta)|E\rangle\langle E|$, the Hamiltonian becomes

$$\widetilde{H}_r = \delta|E\rangle\langle E| + \frac{g\Omega_o}{2\omega_m} a_m^{\dagger}|E\rangle\langle 0| + \frac{g\Omega_o}{2\omega_m} a_m|0\rangle\langle E|, \tag{21}$$

where $\omega_{0E} = \delta + \omega_m + \frac{g^2}{\omega_m} + \omega_o$.

Then we apply another RWA, and set $H_0' = \delta|E\rangle\langle E|$, the Hamiltonian is calculated as

$$\widetilde{H}_r' = \frac{g\Omega_o}{2\omega_m} e^{i\delta t} a_m^{\dagger}|E\rangle\langle 0| + \frac{g\Omega_o}{2\omega_m} e^{-i\delta t} a_m|0\rangle\langle E|. \tag{22}$$

When the interaction strength of $\frac{\Omega_o}{2}$ is far small compared with the detuning δ, the time-average effective Hamiltonian is obtained as [51]

$$\begin{aligned}\widetilde{H}_{eff}' &= \frac{g^2\Omega_o^2}{4\omega_m^2\delta} a_m^{\dagger} a_m(|E\rangle\langle E| - |0\rangle\langle 0|) \\ &\quad - \frac{g^2\Omega_o^2}{4\omega_m^2\delta}|0\rangle\langle 0|.\end{aligned} \tag{23}$$

From the Hamiltonian we can see that the resonant frequency of the phonon crystal will be affected by the state of NVE, which means the resonant frequency shift is proportional to the

Optics EXPRESS

excitation number in state $|0\rangle$. When there is one NV center absorbing a single phonon, the frequency shift of the phonon crystal is

$$\Delta f_s = \frac{g^2\Omega_o^2}{2\omega_m^2\delta}. \tag{24}$$

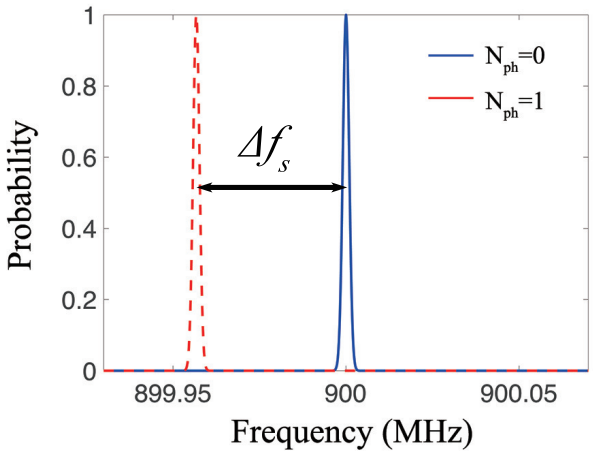

Fig. 3. The schematic diagram of the phonon resonance spectrum with waist width of γ_e. The vertical coordinate represents the probability of a single phonon being absorbed. N_{ph} represents the number of the absorbed phonon. The red line shows that, when there is one single phonon absorbed, the resonance frequency will shift distinctively compared with the non-phonon-absorbed situation.

The effective dissipation of the excited state $|E\rangle$ is $\gamma_e = (\frac{\overline{g}}{\delta})^2\gamma_E$, where $\overline{g} = \frac{g\Omega_o}{2\omega_m}$ is the equivalent coupling strength, γ_E is the decay rate of the energy level $|E\rangle$ with the population of 1. If we set $g = 2\pi\times5MHz, \Omega_o = 2\pi\times290MHz, \omega_m = 2\pi\times900MHz$ [38], $\gamma_E = 2\pi\times3MHz$ [52], and $\delta = 2\pi\times30MHz$, the effective dissipation and the frequency shift can be calculated as $\gamma_e = 2\pi\times2.16kHz$ and $\Delta f_s = 2\pi\times43.26kHz$ respectively, which implies that the single phonon absorption induced frequency shift can be detected distinctively. Without loss of generality, we assume that, the detected phonon absorption spectrum satisfies the Gaussian distribution, the schematic diagram of the detected phonon absorption spectrum is shown in Fig. 3. In fact, as long as we have $\delta \gg \gamma_E$, the demand for the resolution can be satisfied, and the scheme can be realized under the realistic experimental conditions.

5. Dissipation effects

In the above sections, the dynamical evolution has been analysed in ideal condition and the relationship between the driving pulse shape and the emitting phonon shape has been obtained, however, there are various losses in the real systems. If we consider the dynamical evolution of the NVE system with the conditional Hamiltonian which include the possible losses, the whole

Optics EXPRESS

conditional Hamiltonian has the following form:

$$\begin{aligned} H_c &= -i\frac{\gamma_1}{2}|N-1\rangle_{-1}|1\rangle_{+1}|0\rangle_0|0\rangle_m \\ &\quad -i\frac{\gamma_0}{2}|N-1\rangle_{-1}|0\rangle_{+1}|1\rangle_0|0\rangle_m - i\frac{\gamma_m}{2}a_m^\dagger a_m \\ &\quad +g_m(a^\dagger a_m + a a_m^\dagger) + \frac{\Omega(t)}{2}(d^\dagger + d) \\ &\quad +i\sqrt{\kappa/2\pi}\int_{-\Delta\omega_e}^{+\Delta\omega_e} d\omega[a_m^\dagger e(\omega) - a_m e^\dagger(\omega)] \\ &\quad +\int_{-\Delta\omega_e}^{+\Delta\omega_e} d\omega[\omega e^\dagger(\omega)e(\omega)]. \end{aligned} \tag{25}$$

where γ_0 is the dephasing rate in state $|0\rangle$, γ_1 denotes the spontaneous emission of state $|+1\rangle$, and γ_m denotes the phonon dissipation in the single NV evolution.

For numerical simulations, we need to discretize the field $e(\omega)$ by introducing a finite but small frequency interval $\delta\omega$ between two adjacent mode frequencies. Then the number of the total modes we have is $n = \frac{2\Delta\omega_e}{\delta\omega} + 1$, the frequency of the jth mode ω_j which is denoted by e_j is given by $\omega_j = \left(j - \frac{n+1}{2}\right)\delta\omega$. The Hamiltonian can be transformed to the form:

$$\begin{aligned} H_c &= -i\frac{\gamma_1}{2}|N-1\rangle_{-1}|1\rangle_{+1}|0\rangle_0|0\rangle_m \\ &\quad -i\frac{\gamma_0}{2}|N-1\rangle_{-1}|0\rangle_{+1}|1\rangle_0|0\rangle_m - i\frac{\gamma_m}{2}a_m^\dagger a_m \\ &\quad +g_m(a^\dagger a_m + a a_m^\dagger) + \frac{\Omega(t)}{2}(d^\dagger + d) \\ &\quad +i\kappa_e\sum_{j=1}^{n}\sqrt{\delta\omega}[a_m^\dagger e_j - a_m e_j^\dagger] \\ &\quad +\sum_{j=1}^{n}(\omega_j\delta\omega e_j^\dagger e_j), \end{aligned} \tag{26}$$

where $\kappa_e = \sqrt{\kappa\delta\omega/2\pi}$. Similarly, the state $|\Psi\rangle$ of the NVE system can be expanded by the discretized phonon pulse state with the form $|\phi_1\rangle = \sum_{j=1}^{n}\delta\omega b_j e_j^\dagger|vac\rangle$, which is

$$\begin{aligned} |\Psi> &= (c_1|N\rangle_{-1}|0\rangle_{+1}|0\rangle_0|1\rangle_m + c_2|N-1\rangle_{-1}|1\rangle_{+1}|0\rangle_0|0\rangle_m \\ &\quad +c_3|N-1\rangle_{-1}|0\rangle_{+1}|1\rangle_0|0\rangle_m)\otimes|\phi_0\rangle \\ &\quad +|N\rangle_{-1}|0\rangle_{+1}|0\rangle_0|0\rangle_m\otimes|\phi_1\rangle. \end{aligned} \tag{27}$$

Substituting $|\Psi\rangle$ into the schrödinger equation $i\partial_t|\Psi\rangle = H|\Psi\rangle$, we can get

$$\dot{c}_1 = -\frac{\gamma_m}{2}c_1 - ig_m c_2 + \kappa_e\sum_{j=1}^{n}\widetilde{b}_j, \tag{28}$$

$$\dot{c}_2 = -\frac{\gamma_1}{2}c_2 - ig_m c_1 - i\frac{\Omega(t)}{2}c_3, \tag{29}$$

$$\dot{c}_3 = -\frac{\gamma_0}{2}c_3 - i\frac{\Omega(t)}{2}c_2, \tag{30}$$

Optics EXPRESS

$$\dot{b}_j = -\kappa_e c_1 - i\widetilde{b}_j \omega_j, \tag{31}$$

where $\widetilde{b}_j = \sqrt{\delta\omega} b_j$. We assume that, initially, there is a single phonon state in the diamond, which shape is shown as Fig. 2, and all of the NV centers are in the state $|-1\rangle$, which means $c_1 = c_2 = c_3 = 0$, $\sum \left|b_j\right|^2 \neq 0$. If we would like to absorb the phonon effectively, the driving pulse $\Omega'(t)$ should be the time reversal of $\Omega(t)$ in Fig. 2, that is $\Omega'(t) = g_m \exp\left[\kappa\left(-t + \frac{T}{2}\right)/2\right]$, where $T = 20/\kappa$. The shape control of the driving microwave pulse can be easily achieved by modulating an arbitrary wave generator. We set $\gamma_0/2\pi = 0.16kHz$, $\gamma_1/2\pi = 0.16kHz$ [53], $\gamma_m/2\pi = 0.16kHz$ [26, 54], $G_m = 4.8kHz$, $N = 4 \times 10^4$, $g_m/2\pi = 0.96MHz$, and $\kappa/2\pi = 0.32MHz$. The numerical simulation results of absorbing process are shown in Fig. 4(a) with the black lines. Under the condition of strong coupling between the NVE and the phonon, the process is quasi-adiabatic, the value of c_2 is distinctly smaller than c_1 and c_3. The first half is the process that the free single phonon entering the strong coupling area with the NVE plays a leading role, and the latter half is predominantly the absorbing process. at time $t = T$, the fidelity between the actual state and the ideal state is 99.38%. As the dissipations increase, the fidelity decreases obviously which is also shown in Fig. 4(a) with the blue lines. The red lines in Fig. 4(a) implies that, it will also reduce the fidelity of the state if the coupling strength and the effective decay rate κ do not satisfy the adiabatic condition.

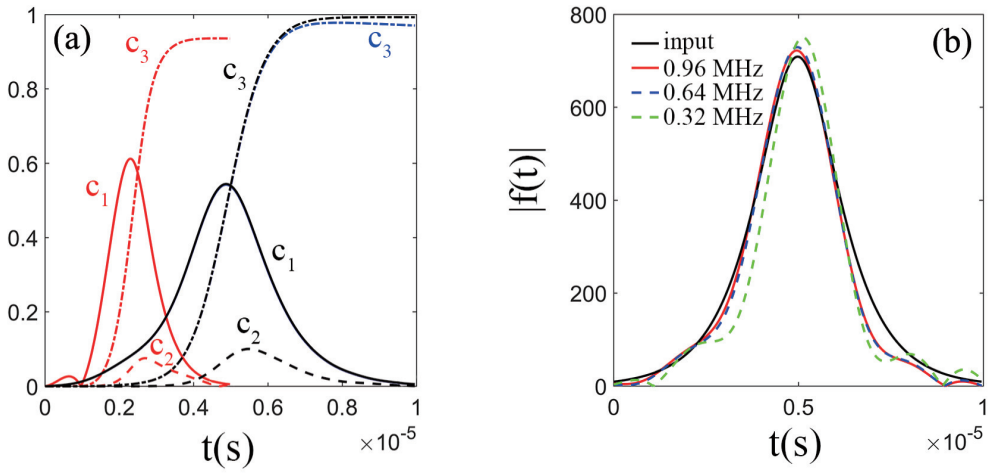

Fig. 4. The numerical simulation results. (a) is the absorbing process. The black lines represent the process with $\gamma_0/2\pi = 0.16kHz$, $\gamma_1/2\pi = 0.16kHz$, $\gamma_m/2\pi = 0.16kHz$, $g_m/2\pi = 0.96MHz$, and $\kappa/2\pi = 0.32MHz$. The blue lines show the process with $\gamma_0/2\pi = 1.6kHz$, $\gamma_1/2\pi = 1.6kHz$, $\gamma_m/2\pi = 1.6kHz$, $g_m/2\pi = 0.96MHz$, and $\kappa/2\pi = 0.32MHz$. The red ones denote the process with $\gamma_0/2\pi = 0.16kHz$, $\gamma_1/2\pi = 0.16kHz$, $\gamma_m/2\pi = 0.16kHz$, $g_m/2\pi = 1.92MHz$, and $\kappa/2\pi = 0.64MHz$. (b) is the emitting process, where the black line represents the input phonon shape, and the red, blue and green lines represent the output phonon shapes when the coupling strength are at $g_m/2\pi = 0.96MHz, 0.64MHz$ and $0.32MHz$ respectively with the same value of $\kappa = 0.32MHz$. The overlap between the input pulse and the output pulse are 98.57%, 98.32% and 94.38% for the red, blue and green lines respectively.

After absorbing and detecting the single phonon, we can apply a driving pulse $\Omega(t)$ on the NVE, the phonon we have just absorbed will then be emitted. The comparison of the input and output

Optics EXPRESS

phonon pulse shape is shown in Fig. 4(b) with the $\kappa = 0.32MHz$. The black line is the input phonon shape, the red, blue and green ones are the output phonon shape with $g_m/2\pi = 0.96MHz$, $0.64MHz$ and $0.32MHz$ respectively. we can see that, the stronger the coupling is, the larger overlap it has between the input and output single phonon shape. When the coupling strength $g_m/2\pi = 0.96MHz$, the overlap can reach 98.57%. In the first step, the NVE absorbs one phonon from the diamond or not. And then, we can detect whether the single phonon state was absorbed through the frequency shift of the phononic crystal. Finally, the NVE can emit the phonon with nearly the same shape compared with the absorbed one. In this process, the single phonon state has been measured without changing the phonon shape, which is a true QND measurement. The process of emitting can act as a single phonon source, it can also be used in the initialization process of the NVE from state $|0\rangle^{\otimes N}$ to state $|-1\rangle^{\otimes N}$. The whole courses including absorbing, detecting and emitting a single phonon can also serve as a single phonon memory.

6. Conclusion

We have proposed a scheme to realize the QND single phonon state detecting and emitting based on the strain mediated interaction between the NVE and the single phonon. By analyze the dynamical evolution of the real system, we are able to calculate the fidelity of the absorbing process and the overlap between the input and output phonon number state, both of which can reach a very high value. The emitting process can act as a single phonon source and the whole courses including absorbing, detecting and emitting a single phonon can also serve as a single phonon memory. In future, the similar method may also be used to realize the QND measurement for arbitrary Fock states of phonons.

Funding

China Postdoctoral Science Foundation (2016M600999); National Natural Science Foundation of China (NSFC) (61435007 and 61771278); Joint Fund of the Ministry of Education of the People's Republic of China (MOE) (6141A02011604); National Natural Science Foundation of China (NSFC) (20141300566).